

# <sup>1</sup> Functional MRI brain state <sup>2</sup> occupancy in the presence of <sup>3</sup> cerebral small vessel disease – a <sup>4</sup> pre-registered replication analysis of <sup>5</sup> the Hamburg City Health Study

✉ For correspondence:

e.schlemm@uke.de

Present address:

Dr. Dr. Eckhard Schlemm,  
Klinik und Poliklinik für  
Neurologie,  
Universitätsklinikum  
Hamburg-Eppendorf,  
Martinistr. 52,  
D-20251 Hamburg

Data availability:

Preprocessed data is  
available on  
<https://github.com/csi-hamburg/HCHS-brain-states-RR>.

Funding: Deutsche  
Forschungsgemeinschaft  
(DFG) – SFB 936,  
178316478 – C2 (Drs  
Thomalla & Cheng)

Competing interests: The  
authors declare no  
competing interests.

<sup>6</sup> Thies Ingwersen, MD  <sup>1</sup>, Carola Mayer, PhD <sup>1</sup>, Marvin Petersen, MD <sup>1</sup>,  
<sup>7</sup> Benedikt M. Frey, MD <sup>1</sup>, Jens Fiehler, MD <sup>2</sup>, Uta Hanning, MD <sup>2</sup>,  
<sup>8</sup> Simone Kühn, PhD <sup>3,4</sup>, Jürgen Gallinat, MD <sup>3</sup>, Raphael Twerenbold,  
<sup>9</sup> MD <sup>5</sup>, Christian Gerloff, MD <sup>6</sup>, Bastian Cheng, MD  <sup>1</sup>, Götz Thomalla,  
<sup>10</sup> MD <sup>1</sup>, Eckhard Schlemm, MBBS PhD  <sup>1</sup>✉

<sup>11</sup> Department of Neurology, University Medical Center

<sup>12</sup> Hamburg-Eppendorf; <sup>2</sup>Department of Neuroradiology, University

<sup>13</sup> Medical Center Hamburg-Eppendorf; <sup>3</sup>Department of Psychiatry,

<sup>14</sup> University Medical Center Hamburg-Eppendorf; <sup>4</sup>Max-Planck-Institut für

<sup>15</sup> Bildungsforschung, Berlin; <sup>5</sup>Department of Cardiology, University

<sup>16</sup> Medical Center Hamburg-Eppendorf; <sup>6</sup>University Medical Center

<sup>17</sup> Hamburg-Eppendorf

<sup>18</sup>

---

## <sup>19</sup> Abstract

<sup>20</sup> **Objective:** To replicate recent findings on the association between the extent of  
<sup>21</sup> cerebral small vessel disease (cSVD), functional brain network dedifferentiation, and  
<sup>22</sup> cognitive impairment.

<sup>23</sup> **Methods:** We analyzed demographic, imaging, and behavioral data from the

<sup>24</sup> prospective population-based Hamburg City Health Study. Using a fully prespecified  
<sup>25</sup> analysis pipeline, we estimated discrete brain states from structural and resting-state  
<sup>26</sup> functional magnetic resonance imaging (MRI). In a multiverse analysis, we varied brain  
<sup>27</sup> parcellations and functional MRI confound regression strategies. The severity of cSVD  
<sup>28</sup> was operationalized as the volume of white matter hyperintensities of presumed  
<sup>29</sup> vascular origin. Processing speed and executive dysfunction were quantified using the  
<sup>30</sup> Trail Making Test (TMT).

<sup>31</sup> **Hypotheses:** We hypothesized a) that a greater volume of supratentorial white matter  
<sup>32</sup> hyperintensities would be associated with less time spent in functional MRI-derived  
<sup>33</sup> brain states of high fractional occupancy; and b) that less time spent in these  
<sup>34</sup> high-occupancy brain states is associated with a longer time to completion in part B of  
<sup>35</sup> the TMT.

<sup>36</sup> **Results:** High-occupancy brain states were characterized by activation or suppression  
<sup>37</sup> of the default mode network. Every 5.1-fold increase in WMH volume was associated  
<sup>38</sup> with a 0.94-fold reduction in the odds of occupying DMN-related brain states ( $P$   
<sup>39</sup>  $5.01 \times 10^{-8}$ ). Every 5 % increase in time spent in high-occupancy brain states was  
<sup>40</sup> associated with a 0.98-fold reduction in the TMT-B completion time ( $P$  0.0116). Findings  
<sup>41</sup> were robust across most brain parcellations and confound regression strategies.

<sup>42</sup> **Conclusion:** We successfully replicated previous findings on the association between  
<sup>43</sup> cSVD, functional brain occupancy, and cognition in an independent sample. The data  
<sup>44</sup> provide further evidence for a functional network dedifferentiation hypothesis of  
<sup>45</sup> cSVD-related cognitive impairment. Further research is required to elucidate the  
<sup>46</sup> mechanisms underlying these associations.

<sup>47</sup> —————

## <sup>48</sup> **Introduction**

<sup>49</sup> Cerebral small vessel disease (cSVD) is an arteriolopathy of the brain associated with age  
<sup>50</sup> and common cardiovascular risk factors (Wardlaw, C. Smith, and Dichgans, 2013). cSVD  
<sup>51</sup> predisposes patients to ischemic stroke (in particular lacunar stroke) and may lead to  
<sup>52</sup> cognitive impairment and dementia (Cannistraro et al., 2019). Neuroimaging findings in  
<sup>53</sup> cSVD reflect its underlying pathology (Wardlaw, Valdés Hernández, and Muñoz-Maniega,  
<sup>54</sup> 2015) and include white matter hyperintensities (WMH), lacunes of presumed vascular  
<sup>55</sup> origin, small subcortical infarcts and microbleeds, enlarged perivascular spaces as well

56 as brain atrophy (Wardlaw, E. E. Smith, et al., 2013). However, the extent of visible cSVD  
57 features on magnetic resonance imaging (MRI) is an imperfect predictor of the severity  
58 of clinical sequelae (Das et al., 2019) and our understanding of the causal mechanisms  
59 linking cSVD-associated brain damage to clinical deficits remains limited (Bos et al., 2018).  
60 Recent efforts have focused on exploiting network aspects of the structural (Tuladhar,  
61 Dijk, et al., 2016; Tuladhar, Tay, et al., 2020; Lawrence, Zeestraten, et al., 2018) and func-  
62 tional (Dey et al., 2016; Schulz et al., 2021) organization of the brain to understand the  
63 relationship between cSVD and clinical deficits in cognition and other domains that rely  
64 on distributed processing. Reduced structural network efficiency has repeatedly been  
65 described as a causal factor in the development of cognitive impairment, particularly  
66 executive dysfunction and reduced processing speed in cSVD (Lawrence, Chung, et al.,  
67 2014; Shen et al., 2020; Reijmer et al., 2016; Prins et al., 2005). Findings with respect  
68 to functional connectivity (FC), however, are more heterogeneous than their SC counter-  
69 parts, perhaps because FC measurements are prone to be affected by hemodynamic  
70 factors and noise, resulting in relatively low reliability, especially with resting-state scans  
71 of short duration (Laumann, Gordon, et al., 2015). This problem is exacerbated in the  
72 presence of cSVD and worsened by arbitrary processing choices (Lawrence, Tozer, et al.,  
73 2018; Gesierich et al., 2020).

74 As a promising new avenue, time-varying, or dynamic, functional connectivity approaches  
75 have recently been explored in patients with subcortical ischemic vascular disease (Yin  
76 et al., 2022; Xu et al., 2021). Although the study of dynamic FC measures may not solve  
77 the problem of limited reliability, especially in small populations or ~~subjects~~participants  
78 with extensive structural brain changes, it adds another – temporal – dimension to the  
79 study of functional brain organization, which is otherwise overlooked. Importantly, FC dy-  
80 namics not only reflect moment-to-moment fluctuations in cognitive processes, but are  
81 also related to brain plasticity and homeostasis (Laumann and Snyder, 2021; Laumann,  
82 Snyder, et al., 2017), which may be impaired in cSVD.

83 In the present paper, we aimed to replicate and extend the main results of (Schlemm  
84 et al., 2022). In this recent study, the authors analyzed MR imaging and clinical data from  
85 the prospective Hamburg City Health Study (HCHS, (Jagodzinski et al., 2020)) using a coac-  
86 tivation pattern approach to define discrete brain states and found associations between  
87 the WMH load, time spent in high-occupancy brain states characterized by activation or  
88 suppression of the default mode network (DMN), and cognitive impairment. Specifically,

89 every 4.7-fold increase in WMH volume was associated with a 0.95-fold reduction in the  
90 odds of occupying a DMN-related brain state; every 2.5 seconds (i.e., one repetition time)  
91 not spent in one of those states was associated with a 1.06-fold increase in TMT-B com-  
92 pletion times.

93 The fractional occupancy of a functional MRI-derived discrete brain state is a **subject-specific**  
94 **participant-specific** measure of brain dynamics and is defined as the proportion of BOLD  
95 volumes assigned to that state relative to all BOLD volumes acquired during a resting-  
96 state scan.

97 Our primary hypothesis for the present work was that the volume of supratentorial  
98 white matter hyperintensities is associated with fractional occupancy of DMN-related  
99 brain states in a middle-aged to elderly population mildly affected by cSVD. Our sec-  
100 ondary hypothesis was that fractional occupancy is associated with executive dysfunc-  
101 tion and reduced processing speed, measured as the time to complete part B of the Trail  
102 Making Test (TMT).

103 Both hypotheses were tested in an independent subsample of the HCHS study popu-  
104 lation using the same imaging protocols, examination procedures, and analysis pipelines  
105 as those in (Schlemm et al., 2022). The robustness of the associations was explored using  
106 a multiverse approach by varying key steps in the analysis pipeline.

## 107 Methods

### 108 Study population

109 This study analyzed data from the Hamburg City Health Study (HCHS), an ongoing prospec-  
110 tive, population-based cohort study aiming to recruit a cross-sectional sample of 45 000  
111 adult participants from the city of Hamburg, Germany (Jagodzinski et al., 2020). From  
112 the first 10 000 participants of the HCHS, we planned to include those who were docu-  
113 mented to have received brain imaging (n=2648) and exclude those who were analyzed  
114 in our previous report (Schlemm et al., 2022) (n=970). The ethical review board of the  
115 Landesärztekammer Hamburg (State of Hamburg Chamber of Medical Practitioners) ap-  
116 proved the HCHS (PV5131), and all participants provided written informed consent.

### 117 Demographic and clinical characterization

118 From the study database, we extracted the participants' age at the time of inclusion in  
119 years, their sex, and the number of years spent in education. During the visit to the study

<sup>120</sup> center, participants underwent cognitive assessment using standardized tests. From the  
<sup>121</sup> database, we extracted their performance scores on the Trail Making Test part B, mea-  
<sup>122</sup> sured in seconds, as an operationalization of executive function and psychomotor pro-  
<sup>123</sup> cessing speed (Tombaugh, 2004; Arbuthnott and Frank, 2000). For descriptive purposes,  
<sup>124</sup> we also extracted data on past medical history and reported the proportion of partici-  
<sup>125</sup> pants with a previous diagnosis of dementia.

## <sup>126</sup> MRI acquisition and preprocessing

<sup>127</sup> The magnetic resonance imaging protocol for the HCHS includes structural and resting-  
<sup>128</sup> state functional sequences. The acquisition parameters for a 3 T Siemens Skyra MRI scan-  
<sup>129</sup> ner (Siemens, Erlangen, Germany) have been previously reported (Petersen et al., 2020;  
<sup>130</sup> Frey et al., 2021) and are given as follows:

<sup>131</sup> For  $T_1$ -weighted anatomical images, a 3D rapid acquisition gradient-echo sequence  
<sup>132</sup> (MPRAGE) was used with the following sequence parameters: repetition time TR = 2500 ms,  
<sup>133</sup> echo time TE = 2.12 ms, 256 axial slices, slice thickness ST = 0.94 mm, and in-plane resolu-  
<sup>134</sup> tion IPR =  $(0.83 \times 0.83) \text{ mm}^2$ .

<sup>135</sup>  $T_2$ -weighted fluid attenuated inversion recovery (FLAIR) images were acquired with  
<sup>136</sup> the following sequence parameters: TR = 4700 ms, TE = 392 ms, 192 axial slices, ST =  
<sup>137</sup> 0.9 mm, IPR =  $(0.75 \times 0.75) \text{ mm}^2$ .

<sup>138</sup> 125 resting state functional MRI volumes were acquired (TR = 2500 ms; TE = 25 ms;  
<sup>139</sup> flip angle = 90°; slices = 49; ST = 3 mm; slice gap = 0 mm; IPR =  $(2.66 \times 2.66) \text{ mm}^2$ ). The  
<sup>140</sup> subjectsparticipants were asked to keep their eyes open and to think of nothing.

<sup>141</sup> We verified the presence and voxel dimensions of expected MRI data for each par-  
<sup>142</sup> ticipant and excluded those for whom at least one of  $T_1$ -weighted, FLAIR, and resting-  
<sup>143</sup> state MRI was missing. We also excluded participants with neuroradiologically confirmed  
<sup>144</sup> space-occupying intra-axial lesion. To ensure reproducibility, no visual quality assess-  
<sup>145</sup> ment of raw images was performed.

<sup>146</sup> For the remaining participants, structural and resting-state functional MRI data was  
<sup>147</sup> preprocessed using FreeSurfer v6.0 (<https://surfer.nmr.mgh.harvard.edu/>), and fmriPrep  
<sup>148</sup> v20.2.6 (Esteban et al., 2019), using default parameters. Participants were excluded if  
<sup>149</sup> automated processing using at least one of these packages failed.

## **150 Quantification of WMH load**

**151** For our primary analysis, the extent of ischemic white matter disease was operational-  
**152** ized as the total volume of supratentorial WMHs obtained from automated segmentation  
**153** using a combination of anatomical priors, BIANCA (Griffanti, Zamboni, et al., 2016), and  
**154** LOCATE (Sundaresan et al., 2019), post-processed with a minimum cluster size of 30 vox-  
**155** els, as described in (Schlemm et al., 2022). In an exploratory analysis, we partitioned  
**156** voxels identified as WMH into deep and periventricular components according to their  
**157** distance to the ventricular system (cut-off 10 mm, (Griffanti, Jenkinson, et al., 2018))

## **158 Brain state estimation**

**159** The output from fMRIprep was post-processed using xcpEngine v1.2.3 to obtain de-confounded  
**160** spatially averaged BOLD time series (Ciric, Wolf, et al., 2017). For the primary analysis, we  
**161** used the  $36p$  regression strategy and the Schaefer-400 parcellation (Schaefer et al., 2018),  
**162** as in (Schlemm et al., 2022).

**163** Different atlases and confound regression strategies, as implemented in xcpEngine,  
**164** were included in an exploratory multiverse analysis.

**165** Co-activation pattern (CAP) analysis was performed by first aggregating parcellated,  
**166** de-confounded BOLD signals into a ( $n_{\text{parcels}} \times \sum_i n_{\text{time points},i}$ ) feature matrix, where  $n_{\text{time points},i}$   
**167** denotes the number of retained volumes for **subject participant**  $i$  after confound regres-  
**168** sion. Clustering was performed using the  $k$ -means algorithm ( $k = 5$ ) with a distance mea-  
**169** sure given by 1 minus the sample Pearson correlation between points, as implemented  
**170** in Matlab R2021a. We estimated the **subject-participant-** and state-specific fractional oc-  
**171** cupancies, which are defined as the proportion of BOLD volumes assigned to each brain  
**172** state (Vidaurre et al., 2018). The two states with the highest average occupancies were  
**173** identified as the basis for further analysis.

## **174 Statistical analysis**

**175** For demographic (age, sex, and years of education) and clinical (TMT-B) variables, the  
**176** number of missing items is reported. For non-missing values, we provide descriptive  
**177** summary statistics using median and interquartile range. The proportions of men and  
**178** women in the sample are reported. Since we expected based on our pilot data (Schlemm  
**179** et al., 2022) that the proportion of missing data would be small, primary regression mod-  
**180** elling was carried out as a complete-case analysis.

181 As an outcome-neutral quality check of the implementation of the MRI processing  
182 pipeline, brain state estimation, and co-activation pattern analysis, we compared frac-  
183 tional occupancies between brain states. We expected that the average fractional oc-  
184 cupancy in the two high-occupancy states would be higher than the average fractional  
185 occupancy in the other three states. Point estimates and 95% confidence intervals are  
186 presented for the difference in average fractional occupancy to verify this assertion.

187 For further analyses, non-zero WMH volumes were subjected to logarithmic transfor-  
188 mation. Zero values retained their value of zero; to compensate, all models included a  
189 binary indicator for zero WMH volume if at least one non-zero WMH value was present.

190 To assess the primary hypothesis of a negative association between the extent of  
191 ischemic white matter disease and time spent in high-occupancy brain states, we per-  
192 formed a fixed-dispersion Beta regression to model the logit of the conditional expec-  
193 tation of the average fractional occupancy of two high-occupancy states as an affine  
194 function of the logarithmized WMH load. Age and sex were included as covariates. The  
195 strength of the association was quantified as the odds ratio per interquartile ratio of the  
196 WMH burden distribution, and is accompanied by a 95% confidence interval. Significance  
197 testing of the null hypothesis of no association was conducted at the conventional signif-  
198 icance level of 0.05. Estimation and testing were carried out using the 'betareg' package  
199 v3.1.4 in R v4.2.1.

200 To assess the secondary hypothesis of an association between time spent in high-  
201 occupancy brain states and executive dysfunction, we performed a generalized linear  
202 regression with a Gamma response distribution to model the logarithm of the condi-  
203 tional expected completion time in part B of the TMT as an affine function of the average  
204 fractional occupancy of two high-occupancy states. Age, sex, years of education, and  
205 logarithmized WMH load were included as covariates. The strength of the association  
206 was quantified as a multiplicative factor per percentage point and accompanied by a  
207 95% confidence interval. Significance testing of the null hypothesis of no association was  
208 conducted at the conventional significance level of 0.05. Estimation and testing were  
209 performed using the glm function included in the 'stats' package from R v4.2.1.

## 210 Pre-registered analyses

211 The analysis plan was [pre-registered](#) on June 27 2023 at [https://osf.io/](https://osf.io/fcqmb)  
212 [fcqmb](#). The sample size calculation was based on an effect size on the odds ratio scale of  
213 0.95, corresponding to an absolute difference in the probability of occupying a DMN-

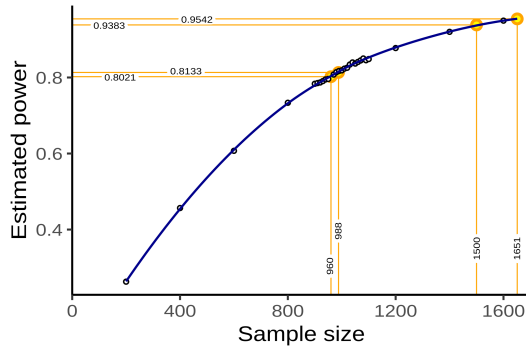


**Figure 1 | Sample size and power estimation.** A-priori estimated power for different sample sizes was obtained as the proportion of synthetic data sets in which the null hypothesis of no association between WMH volume and time spent in high-occupancy brain states can be rejected at the  $\alpha = 0.05$  significance level. Proportions are based on a total of 10 000 synthetic data sets obtained by bootstrapping the data presented in (Schlemm et al., 2022). Highlighted in orange are the smallest sample size ensuring a power of at least 80 % ( $n = 960$ ), the sample size of the pilot data ( $n = 988$ , post-hoc power 81.3 %), the expected sample size for this replication study ( $n = 1500$ , a-priori power 93.9 %), and the achieved sample size ( $n = 1651$ , a-priori power 95.4 %).

related brain state between the first and third WMH-load quartile of 1.3 percentage points, and between the 5% and 95% percentile of 3.1 percentage points. Approximating half the difference in fractional occupancy of DMN-related states between different task demands (rest vs n-back) in healthy subjects, which was estimated to lie between 6 and 7 percentage points (Cornblath et al., 2020), this value represented a plausible choice for the smallest effect size of theoretical and practical interest. It also equals the estimated effect size based on the data presented in (Schlemm et al., 2022).

Simple bootstrapping was used to create 10 000 hypothetical datasets of size 200, 400, 600, 800, 900, 910, ..., 1090, 1100, 1200, 1400, 1500, and 1600. Each dataset was then subjected to the estimation procedure described above. For each sample size, the proportion of datasets in which the primary null hypothesis of no association between fractional occupancy and WMH load could be rejected at  $\alpha = 0.05$  was computed and recorded as a power curve in Figure 1.

A sample size of 960 would have allowed the replication of the reported effect with a power of 80.2 %. We had anticipated a sample size of 1500, which would have yielded a power of 93.9 %.

## Multiverse analysis

In both (Schlemm et al., 2022) and our primary replication analysis, we made certain analytical choices in the operationalization of brain states and ischemic white matter disease, namely the use of the 36p confound regression strategy, the Schaefer-400 parcellation,

234 and a BIANCA/LOCATE-based WMH segmentation algorithm. The robustness of the as-  
235 sociation between WMH burden and time spent in high-occupancy states with regard to  
236 other choices was explored in a multiverse analysis (Steegen et al., 2016). Specifically, in  
237 an exploratory analysis, we estimated brain states from BOLD time series processed ac-  
238 cording to a variety of established confound regression strategies and aggregated over  
239 different cortical brain parcellations (Table 2, Ceric, Rosen, et al., 2018; Ceric, Wolf, et al.,  
240 2017). The extent of cSVD was additionally quantified by the volume of deep and periven-  
241 tricular white matter hyperintensities.

242 For each combination of analytical choice of confound regression strategy, parcella-  
243 tion, and subdivision of white matter lesion load ( $9 \times 9 \times 3 = 243$  scenarios in total), we  
244 quantified the association between WMH load and average time spent in high-occupancy  
245 brain states using odds ratios and 95 % confidence intervals as described above.

246 No hypothesis testing was performed for these multiverse analyses. Rather, they  
247 serve to inform about the robustness of the outcome of the test of the primary hypoth-  
248 esis. Any substantial conclusions about the association between the severity of cerebral  
249 small vessel pathology and the time spent in high-occupancy brain states were drawn  
250 from the primary analysis using pre-specified methodological choices, as stated in the  
251 Scientific Question in Table 1.

## 252 **Further exploratory analysis**

253 In previous work, two high-occupancy brain states have been related to the default mode  
254 network (Cornblath et al., 2020). We further explored this relationship by computing, for  
255 each individual brain state, the cosine similarity of the positive and negative activations of  
256 the cluster's centroid with a set of a priori defined functional 'communities' or networks  
257 (Schaefer et al., 2018; Yeo et al., 2011). The results were visualized as spider plots for the  
258 Schaefer atlases.

259 In further exploratory analyses, we describe the associations between brain state dy-  
260 namics and other measures of cognitive ability such as memory and language.

## 261 **Pilot data and analysis**

262 Summary data from the first 1000 imaging data points of the HCHS have been published  
263 with (Schlemm et al., 2022) and formed the basis for the hypotheses tested in this replication  
264 study. Before pre-registration, we had implemented our prespecified analysis pipeline described  
265 above in R and Matlab, and applied it to this previous sample. Data, code and results

<sup>266</sup> from this pilot analysis have been stored with the archived Stage 1 report on GitHub  
<sup>267</sup> ([https://github.com/csi-hamburg/HCHS\\_brain\\_states\\_RR\\_v1.5](https://github.com/csi-hamburg/HCHS_brain_states_RR_v1.5)) and preserved on Zenodo.

## <sup>268</sup> Timeline and access to data

<sup>269</sup> At the time of planning of this study, all demographic, clinical and imaging data used in  
<sup>270</sup> this analysis had been collected by the HCHS and were held in the central trial database.  
<sup>271</sup> Quality checks for non-imaging variables had been performed centrally. WMH segmentation  
<sup>272</sup> based on structural MRI data of the first 10 000 participants of the HCHS had been performed  
<sup>273</sup> previously using the BIANCA/LOCATE approach (Rimmele et al., 2022). Functional MRI  
<sup>274</sup> data and clinical measures of executive dysfunction (TMT-B scores) had not previously  
<sup>275</sup> been analyzed by the pre-registering author (ES).

## <sup>276</sup> Deviations from preregistration

<sup>277</sup> For deconfounding and aggregating BOLD data at brain parcellation level, the software  
<sup>278</sup> xcpEngine was used in version 1.2.3, not 1.2.1, to ensure that the correct MNI ref-  
<sup>279</sup> erence template (MNI152NLin2009cAsym) is used for registration of brain atlases. This  
<sup>280</sup> decision was made before analysing the data.

## <sup>281</sup> Results

<sup>282</sup> For this replication study, a total of 2648 datasets were available, of which 970 were al-  
<sup>283</sup> ready included in our previous analysis and thus discarded. In 13 of the resulting 1678  
<sup>284</sup> datasets, one or more MRI sequences were missing. Of the complete datasets (n=1665),  
<sup>285</sup> we excluded 5 participants due to intra-axial space-occupying lesions. An additional 9  
<sup>286</sup> subjects-participants were excluded because of unsuccessful preprocessing, WMH seg-  
<sup>287</sup> mentation, or xcpEngine failure, resulting in 1651 datasets for analysis. A study-flowchart  
<sup>288</sup> is provided in Figure 2.

<sup>289</sup> Baseline demographic and cognitive values, including the number of missing items,  
<sup>290</sup> are reported in Table 4.

<sup>291</sup> WMH volumes (median 1.05 mL, IQR 0.47 mL to 2.37 mL), motion estimates, and frac-  
<sup>292</sup> tional occupancies of brain states 1 through 5 are reported in Table 5.

<sup>293</sup> In an outcome-neutral quality check of the implementation of (i) the MRI processing  
<sup>294</sup> pipeline, (ii) brain state estimation, and (iii) co-activation pattern analysis, the mean differ-  
<sup>295</sup> ence in fractional occupancy between high- and low-occupancy states was consistently

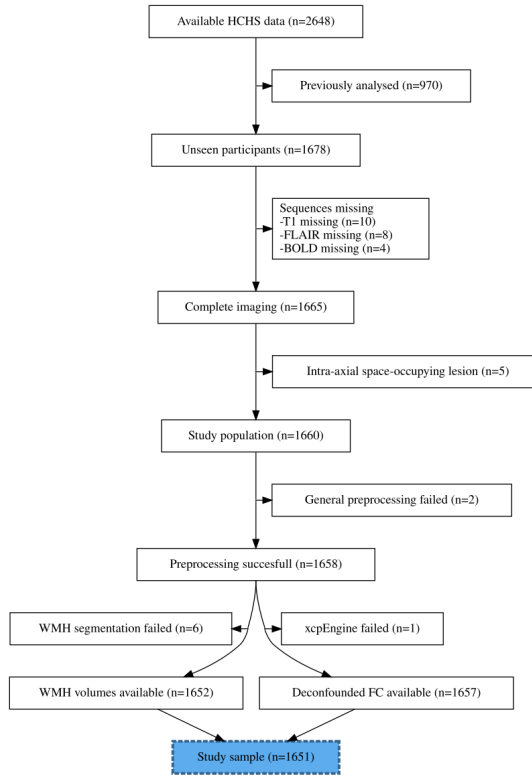


**Figure 2 | Study flowchart.** Composition of the study population after application of inclusion and exclusion criteria, and image processing.

296 maintained, with a point-estimate of the separation between two high-occupancy and  
 297 three low-occupancy states of 6.7 % (95 % confidence interval, 6.2 % to 7.1 %) in the 36p  
 298 paradigm. This indicates that the implementation of the pipeline was correct and that  
 299 the brain state estimation and co-activation pattern analysis worked as intended.

### 300 Pre-registered hypotheses

#### 301 Association between WMH load and fractional occupancy

302 The results of the test of our primary preregistered hypothesis of an association be-  
 303 tween supratentorial WMH volume and the time spent in high-occupancy brain states  
 304 are shown in Figure 3 and Table 7.

305 Adjusted for age and sex, there was a 0.94-fold reduction in the odds of occupying a  
 306 high-occupancy brain state for every 5.1-fold increase in WMH load ( $P 5.01 \times 10^{-8}$ ).

#### 307 Association between executive function and fractional occupancy in DMN- 308 related states

309 The results of the test of our secondary preregistered hypothesis of an association be-  
 310 tween time spent in high-occupancy brain states and executive function as measured by

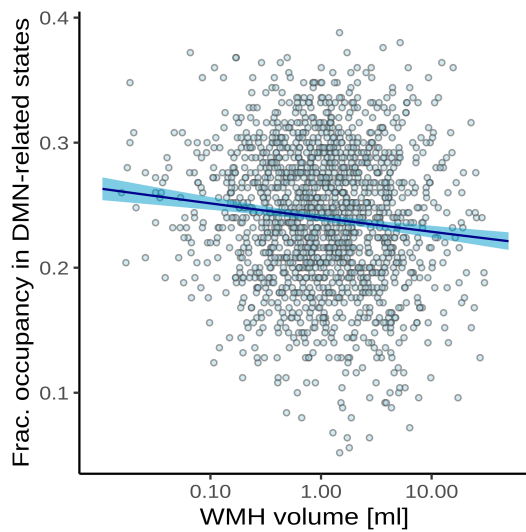


**Figure 3 | Association between time spent in high-occupancy brain states and supratentorial WMH volume.** Point estimates (black line) and 95%-confidence region (light blue ribbon) of the conditional mean fractional occupancy are obtained from unadjusted beta regression modelling. Each marker represents one of N=1642 independent participants with a non-zero total WMH volume.

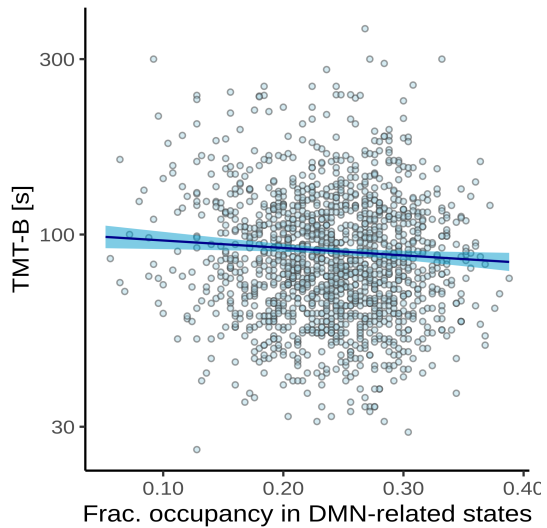


**Figure 4 | Association between time spent in high-occupancy DMN-related brain states and TMT-B completion time.** Point estimates (black line) and 95%-confidence region (light blue ribbon) of the conditional mean TMT-B completion time are obtained from unadjusted Gamma regression modelling. Each marker represent one of N=1482 independent participants with non-zero total WMH volume and available TMT-B data.

<sup>327</sup> icant negative and no significant positive associations, irrespective of operationalization  
<sup>328</sup> of cSVD (total vs. periventricular vs. deep WMH volume) (Figure 5B).

### <sup>329</sup> Additional analyses

<sup>330</sup> Connectivity profiles of brain states – relation to default mode network  
<sup>331</sup> Based on the cosine similarity between positive and negative activations of cluster cen-  
<sup>332</sup> troids and indicator vectors of pre-defined large scale brain networks, network activation  
<sup>333</sup> profiles were computed for brain states estimated from Schaefer parcellations of varying  
<sup>334</sup> spatial resolutionresolutions.

<sup>335</sup> Figure 6 shows the corresponding spider plots, identifying states characterized by  
<sup>336</sup> activation (DMN+) or suppression (DMN-) of the default mode network as states with the  
<sup>337</sup> highest fractional occupancy.

### <sup>338</sup> Association with other cognitive domains

<sup>339</sup> Associations between the time spent in high-occupancy DMN-related brain states and  
<sup>340</sup> cognitive measures beyond TMT-B are shown in Figure 7.

<sup>341</sup> Adjusted for age, sex, WMH load, and years of education, FO in DMN-related states  
<sup>342</sup> appeared to be associated with better word recall (aORadjusted OR 1.19, nominal P  
<sup>343</sup> 0.013), but not with global cognitive functioning (MMSE, aORadjusted OR 1.09) or vocab-  
<sup>344</sup> ular (aOR 1.09), nor with verbal fluency (animal naming, adjusted  $\exp(\beta)$  1.04), or pure  
<sup>345</sup> processing speed (TMT-A, adjusted  $\exp(\beta)$  0.97).

## <sup>346</sup> Summary and Discussion

<sup>347</sup> In this pre-registered cross-sectional study we replicated the key findings of Schlemm  
<sup>348</sup> et al., 2022 in an independent population-based sample of 1651 middle-aged to elderly  
<sup>349</sup> participants of the Hamburg City Health Study.

<sup>350</sup> First, we confirmed that the severity of cerebral small vessel disease is associated with  
<sup>351</sup> the time spent in high-occupancy brain states, defined by functional MRI. More precisely,  
<sup>352</sup> we showed that every 5.1-fold increase in the volume of supratentorial white matter hy-  
<sup>353</sup> perintensities of presumed vascular origin (WMH) was associated with a 0.95-fold reduc-  
<sup>354</sup> tion in the odds of occupying a brain state characterized by activation or suppression of  
<sup>355</sup> the default-mode network, at any given time during the resting-state scan.

<sup>356</sup> Second, we confirmed that the time spent in high-occupancy brain states at rest is  
<sup>357</sup> associated with cognitive performance. More precisely, a 5%-reduction in the fractional

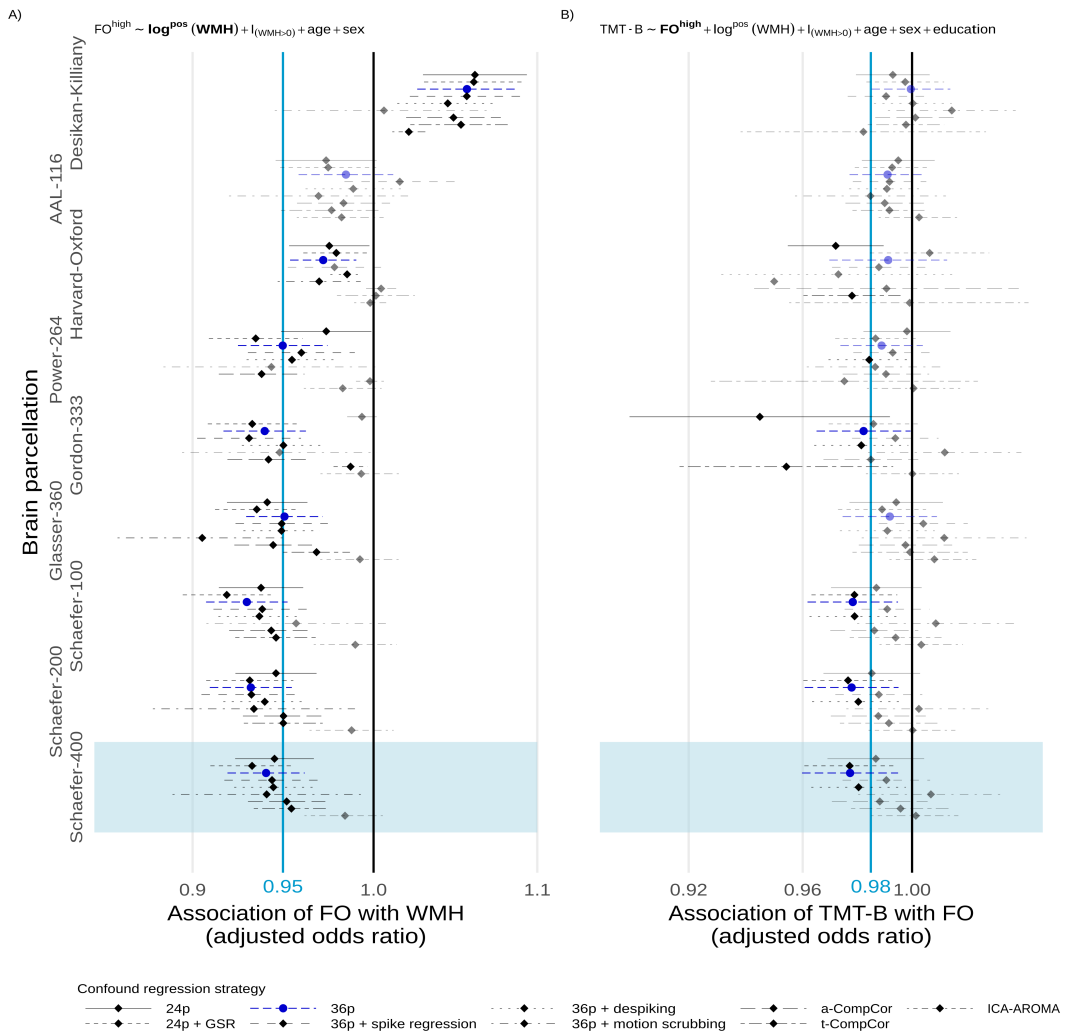


**Figure 5 | Multiverse analysis.** Adjusted effect size estimates of the associations between cSVD severity (WMH volume) and network dedifferentiation (less time spent in high-occupancy DMN-related brain states) [A]), and between network dedifferentiation and executive function (TMT-B completion time) [B]). Effect sizes are given per 5.1-fold increase in WMH volume and a 5%-increase in fractional occupancy, respectively. Markers and line segments indicate point estimates and 95%-confidence intervals for adjusted odds ratios for different combinations of confound regression strategy and brain parcellation. The primary analytical choices are indicated by dark blue circles (36p) and light blue shading (Schaefer-400). Model equations for beta and gamma regressions, respectively, are given at the top. Vertical lines indicate no effect (black) and the effect size observed in the discovery cohort (Schlemm et al., 2022) (light blue), respectively, for reference. Effect sizes not reaching nominal statistical significance ( $\alpha = 0.05$ ) are shown desaturated. Corresponding data based on periventricular and deep WMH volumes are presented in the Supplementary Appendix.

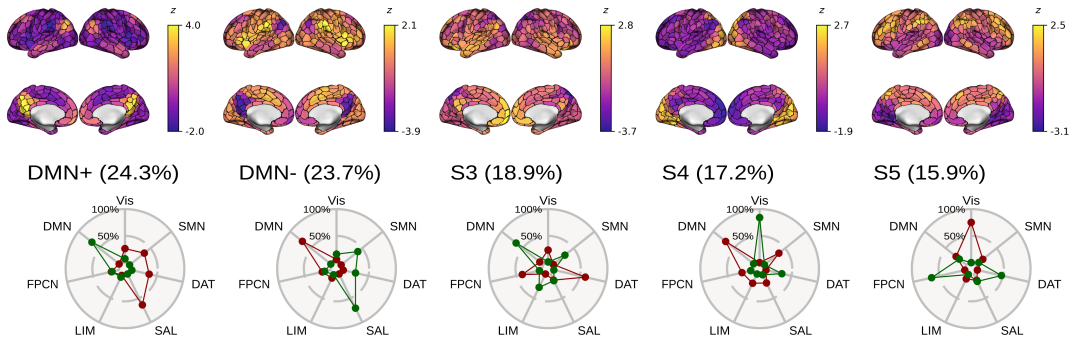


**Figure 6 | Connectivity profiles of brain states.** [Top] Centroids of each identified brain state visualized in brain space. Note the individual color scales. [Bottom] Cosine similarity between centroids of brain states and signed indicator vectors corresponding to activation (green) and suppression (red) of each of seven predefined large-scale functional brain networks (Yeo et al., 2011).

States are ordered by mean fractional occupancy across N=1651 independent participants, indicated by parenthetical percentages. Two high-occupancy states are characterized by activation or suppression of the DMN, the remaining three low-occupancy states (S3–5) were not used in the present study. Note that mean FO values are similar, but not identical, to median FO values reported in Table 5.

occupancy of DMN-related brain states was associated with a 1.02-fold increase in the time to complete part B of the trail making test (TMT).

In a pre-planned multiverse analysis, [these findings](#) [findings relating to our primary and, to a lesser extent, secondary hypotheses](#) were robust with respect to variations in brain parcellations and confound regression strategies. Inconsistent results were found with the Desikan–Killiany parcellation, likely reflecting the notion that the spatial resolution and functional specificity of this coarse, structurally defined atlas are inadequate for analyzing functionally defined brain states. Across brain parcellations, effect sizes were smaller with the ICA-AROMA confound regression strategy and failed to reach nominal statistical significance. This might be due to a relatively large residual motion component in measures of dynamical functional Connectivity after de-noising with ICA-AROMA, as described previously (Lydon-Staley et al., 2019).

We also confirmed across several brain parcellation resolutions that high-occupancy states at rest are characterized by either activation or suppression of the default mode network, reflecting its role as the predominant task-negative brain network.

In unplanned, exploratory analyses, we described the association between brain state dynamics and cognitive measures other than executive function and processing speed and reported a strong, preliminary association between time spent in high-occupancy states and delayed word recall.

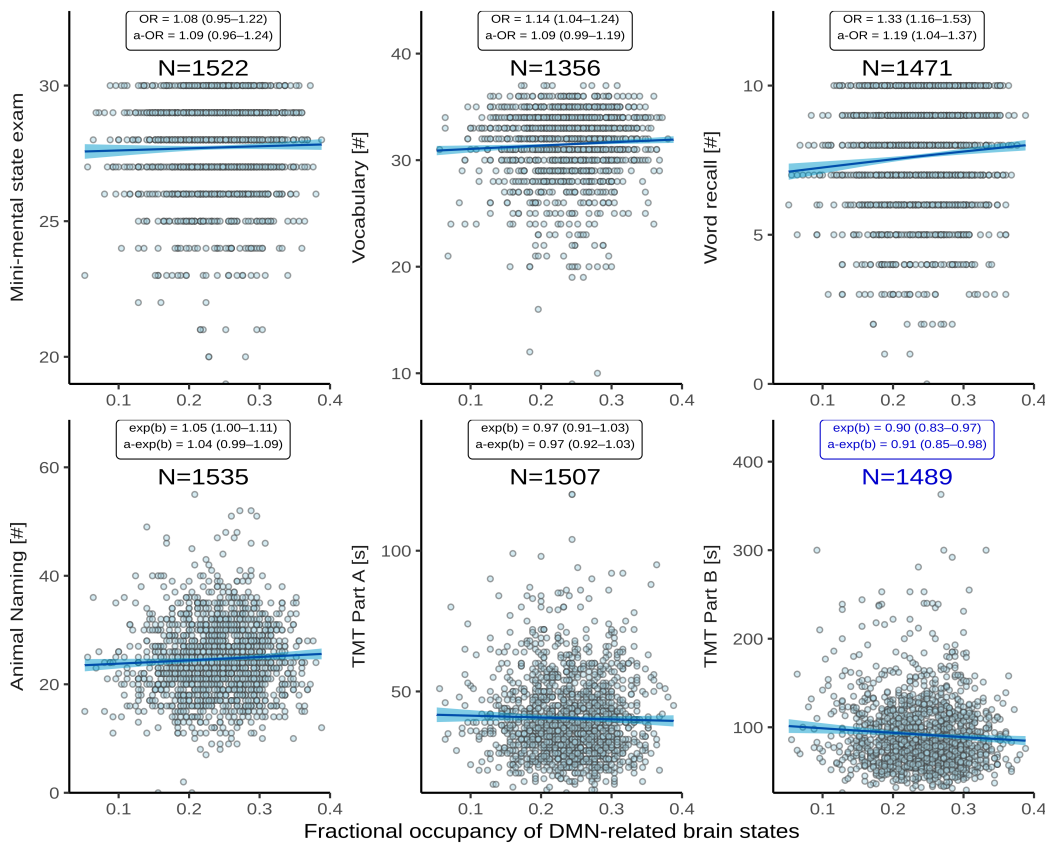


**Figure 7 | Association between time spent in high-occupancy DMN-related brain states and cognitive measures.** Point estimates (black line) and 95%-confidence region (light blue ribbon) of the conditional mean cognitive measures are obtained from unadjusted binomial (top row: Mini-Mental State Examination, Vocabulary, Word List Recall, logit link) and Gamma regression (bottom row: Animal Naming, Trail Making Test [TMT] A/B: log link) modelling. Each marker represents one of N independent participants, as indicated. Insets report effect sizes and P-values both with (adjusted [a-]) and without adjustment for the nuisance variables age, sex, WMH volume (coded as in Figure 5), and years of education. Effect sizes were quantified as odds ratios (ORs) (top) or response scale multipliers [exp(b)] (bottom), and correspond to a 20%-increase in fractional occupancy. Note the different reference change in FO compared to Table 9 chosen to adequately represent some of the smaller effect sizes. The bottom right panel highlighted in dark blue reproduces Figure 4.

<sup>377</sup> We further explored, ~~but did not report in detail~~ and report in the Supplementary  
<sup>378</sup> appendix, the effect of motion; ~~all reported associations~~ results relating to our primary  
<sup>379</sup> and, to a lesser extent, secondary, hypotheses were robust to additional, unplanned ad-  
<sup>380</sup> justments for DVARS, RMSD or, and mean framewise displacement.

<sup>381</sup> The presented results provide robust evidence for a behaviorally relevant association  
<sup>382</sup> between cerebral small vessel disease and functional brain network dedifferentiation.

<sup>383</sup> Further research is required to replicate our findings in different populations, such  
<sup>384</sup> as those affected more severely by cSVD or cognitive impairment, or being studied using  
<sup>385</sup> different imaging protocols, to determine the generalizability of our findings with respect  
<sup>386</sup> to varying operationalizations of the notions of cSVD, brain state, and cognition, and to  
<sup>387</sup> understand the mechanisms underlying the reported associations.

### <sup>388</sup> **Timeline and access to data**

<sup>389</sup> At the time of planning of this study, all demographic, clinical and imaging data used in  
<sup>390</sup> this analysis had been collected by the HCHS and were held in the central trial database.  
<sup>391</sup> Quality checks for non-imaging variables had been performed centrally. WMH segmentation  
<sup>392</sup> based on structural MRI data of the first 10 000 participants of the HCHS had been performed  
<sup>393</sup> previously using the BIANCA/Locate approach. Functional MRI data and clinical measures  
<sup>394</sup> of executive dysfunction (TMT-B scores) had not previously been analyzed by the pre-registering  
<sup>395</sup> author (ES).

### <sup>396</sup> **Acknowledgment**

<sup>397</sup> This preprint was created using the LaPreprint template (<https://github.com/roaldarbol/lapreprint>) by Mikkel Roald-Arbøl .

### <sup>399</sup> **Disclosure**

<sup>400</sup> The authors of this article declare that they have no financial conflict of interest with the  
<sup>401</sup> content of this article.

### <sup>402</sup> **References**

<sup>403</sup> Arbuthnott, Katherine and Janis Frank (2000). "Trail making test, part B as a measure of  
<sup>404</sup> executive control: validation using a set-switching paradigm". In: *Journal of clinical and*  
<sup>405</sup> *experimental neuropsychology* 22.4, pp. 518–528.

- <sup>406</sup> Behzadi, Yashar et al. (2007). "A component based noise correction method (CompCor)  
<sup>407</sup> for BOLD and perfusion based fMRI". In: *Neuroimage* 37.1, pp. 90–101.
- <sup>408</sup> Bos, Daniel et al. (2018). "Cerebral small vessel disease and the risk of dementia: A sys-  
<sup>409</sup> tematic review and meta-analysis of population-based evidence". en. In: *Alzheimers.*  
<sup>410</sup> *Dement.* 14.11, pp. 1482–1492.
- <sup>411</sup> Cannistraro, Rocco J et al. (2019). "CNS small vessel disease: A clinical review". en. In: *Neu-  
rology* 92.24, pp. 1146–1156.
- <sup>413</sup> Ceric, Rastko, Adon FG Rosen, et al. (2018). "Mitigating head motion artifact in functional  
<sup>414</sup> connectivity MRI". In: *Nature protocols* 13.12, pp. 2801–2826.
- <sup>415</sup> Ceric, Rastko, Daniel H Wolf, et al. (2017). "Benchmarking of participant-level confound  
<sup>416</sup> regression strategies for the control of motion artifact in studies of functional con-  
<sup>417</sup> nectivity". en. In: *Neuroimage* 154, pp. 174–187.
- <sup>418</sup> Cornblath, Eli J et al. (2020). "Temporal sequences of brain activity at rest are constrained  
<sup>419</sup> by white matter structure and modulated by cognitive demands". en. In: *Commun Biol*  
<sup>420</sup> 3.1, p. 261.
- <sup>421</sup> Cox, Robert W (1996). "AFNI: software for analysis and visualization of functional mag-  
<sup>422</sup> netic resonance neuroimages". In: *Computers and Biomedical research* 29.3, pp. 162–  
<sup>423</sup> 173.
- <sup>424</sup> Das, Alvin S et al. (2019). "Asymptomatic Cerebral Small Vessel Disease: Insights from  
<sup>425</sup> Population-Based Studies". en. In: *J. Stroke Cerebrovasc. Dis.* 21.2, pp. 121–138.
- <sup>426</sup> Desikan, Rahul S et al. (2006). "An automated labeling system for subdividing the human  
<sup>427</sup> cerebral cortex on MRI scans into gyral based regions of interest". In: *Neuroimage* 31.3,  
<sup>428</sup> pp. 968–980.
- <sup>429</sup> Dey, Ayan K et al. (2016). "Pathoconnectomics of cognitive impairment in small vessel  
<sup>430</sup> disease: A systematic review". en. In: *Alzheimers. Dement.* 12.7, pp. 831–845.
- <sup>431</sup> Esteban, Oscar et al. (2019). "fMRIprep: a robust preprocessing pipeline for functional  
<sup>432</sup> MRI". en. In: *Nat. Methods* 16.1, pp. 111–116.
- <sup>433</sup> Frey, Benedikt M et al. (2021). "White matter integrity and structural brain network topol-  
<sup>434</sup> ogy in cerebral small vessel disease: The Hamburg city health study". en. In: *Hum. Brain*  
<sup>435</sup> *Mapp.* 42.5, pp. 1406–1415.
- <sup>436</sup> Friston, Karl J et al. (1996). "Movement-related effects in fMRI time-series". In: *Magnetic*  
<sup>437</sup> *resonance in medicine* 35.3, pp. 346–355.

- <sup>438</sup> Gesierich, Benno et al. (2020). "Alterations and test-retest reliability of functional connec-  
<sup>439</sup> tivity network measures in cerebral small vessel disease". en. In: *Hum. Brain Mapp.*  
<sup>440</sup> 41.10, pp. 2629–2641.
- <sup>441</sup> Glasser, Matthew F et al. (2016). "A multi-modal parcellation of human cerebral cortex".  
<sup>442</sup> en. In: *Nature* 536.7615, pp. 171–178.
- <sup>443</sup> Gordon, Evan M et al. (2016). "Generation and Evaluation of a Cortical Area Parcellation  
<sup>444</sup> from Resting-State Correlations". en. In: *Cereb. Cortex* 26.1, pp. 288–303.
- <sup>445</sup> Griffanti, Ludovica, Mark Jenkinson, et al. (2018). "Classification and characterization of  
<sup>446</sup> periventricular and deep white matter hyperintensities on MRI: A study in older adults".  
<sup>447</sup> en. In: *Neuroimage* 170, pp. 174–181.
- <sup>448</sup> Griffanti, Ludovica, Giovanna Zamboni, et al. (2016). "BIANCA (Brain Intensity AbNormal-  
<sup>449</sup> ity Classification Algorithm): A new tool for automated segmentation of white matter  
<sup>450</sup> hyperintensities". en. In: *Neuroimage* 141, pp. 191–205.
- <sup>451</sup> Jagodzinski, Annika et al. (2020). "Rationale and Design of the Hamburg City Health Study".  
<sup>452</sup> en. In: *Eur. J. Epidemiol.* 35.2, pp. 169–181.
- <sup>453</sup> Laumann, Timothy O, Evan M Gordon, et al. (2015). "Functional system and areal organi-  
<sup>454</sup> zation of a highly sampled individual human brain". In: *Neuron* 87.3, pp. 657–670.
- <sup>455</sup> Laumann, Timothy O and Abraham Z Snyder (2021). "Brain activity is not only for thinking".  
<sup>456</sup> In: *Current Opinion in Behavioral Sciences* 40, pp. 130–136.
- <sup>457</sup> Laumann, Timothy O, Abraham Z Snyder, et al. (2017). "On the stability of BOLD fMRI  
<sup>458</sup> correlations". In: *Cerebral cortex* 27.10, pp. 4719–4732.
- <sup>459</sup> Lawrence, Andrew J, Ai Wern Chung, et al. (2014). "Structural network efficiency is as-  
<sup>460</sup> sociated with cognitive impairment in small-vessel disease". en. In: *Neurology* 83.4,  
<sup>461</sup> pp. 304–311.
- <sup>462</sup> Lawrence, Andrew J, Daniel J Tozer, et al. (2018). "A comparison of functional and trac-  
<sup>463</sup> tography based networks in cerebral small vessel disease". en. In: *Neuroimage Clin* 18,  
<sup>464</sup> pp. 425–432.
- <sup>465</sup> Lawrence, Andrew J, Eva A Zeestraten, et al. (2018). "Longitudinal decline in structural  
<sup>466</sup> networks predicts dementia in cerebral small vessel disease". en. In: *Neurology* 90.21,  
<sup>467</sup> e1898–e1910.
- <sup>468</sup> Lydon-Staley, David M et al. (2019). "Evaluation of confound regression strategies for  
<sup>469</sup> the mitigation of micromovement artifact in studies of dynamic resting-state func-

- 470 tional connectivity and multilayer network modularity". In: *Network Neuroscience* 3.2,  
471 pp. 427–454.
- 472 Macey, Paul M et al. (2004). "A method for removal of global effects from fMRI time series".  
473 In: *Neuroimage* 22.1, pp. 360–366.
- 474 Makris, Nikos et al. (2006). "Decreased volume of left and total anterior insular lobule in  
475 schizophrenia". In: *Schizophrenia research* 83.2-3, pp. 155–171.
- 476 Muschelli, John et al. (2014). "Reduction of motion-related artifacts in resting state fMRI  
477 using aCompCor". In: *Neuroimage* 96, pp. 22–35.
- 478 Petersen, Marvin et al. (2020). "Network Localisation of White Matter Damage in Cerebral  
479 Small Vessel Disease". en. In: *Sci. Rep.* 10.1, p. 9210.
- 480 Power, Jonathan D, Alexander L Cohen, et al. (2011). "Functional network organization of  
481 the human brain". en. In: *Neuron* 72.4, pp. 665–678.
- 482 Power, Jonathan D, Anish Mitra, et al. (2014). "Methods to detect, characterize, and re-  
483 move motion artifact in resting state fMRI". In: *Neuroimage* 84, pp. 320–341.
- 484 Prins, Niels D et al. (2005). "Cerebral small-vessel disease and decline in information pro-  
485 cessing speed, executive function and memory". en. In: *Brain* 128.Pt 9, pp. 2034–2041.
- 486 Pruim, Raimon HR et al. (2015). "ICA-AROMA: A robust ICA-based strategy for removing  
487 motion artifacts from fMRI data". In: *Neuroimage* 112, pp. 267–277.
- 488 Reijmer, Yael D et al. (2016). "Small vessel disease and cognitive impairment: The rele-  
489 vance of central network connections". en. In: *Hum. Brain Mapp.* 37.7, pp. 2446–2454.
- 490 Rimmele, David Leander et al. (2022). "Association of Carotid Plaque and Flow Velocity  
491 With White Matter Integrity in a Middle-aged to Elderly Population". en. In: *Neurology*.
- 492 Satterthwaite, Theodore D et al. (2013). "An improved framework for confound regres-  
493 sion and filtering for control of motion artifact in the preprocessing of resting-state  
494 functional connectivity data". In: *Neuroimage* 64, pp. 240–256.
- 495 Schaefer, Alexander et al. (2018). "Local-Global Parcellation of the Human Cerebral Cortex  
496 from Intrinsic Functional Connectivity MRI". en. In: *Cereb. Cortex* 28.9, pp. 3095–3114.
- 497 Schlemm, Eckhard et al. (2022). "Equalization of Brain State Occupancy Accompanies  
498 Cognitive Impairment in Cerebral Small Vessel Disease". en. In: *Biol. Psychiatry* 92.7,  
499 pp. 592–602.
- 500 Schulz, Maximilian et al. (2021). "Functional connectivity changes in cerebral small vessel  
501 disease - a systematic review of the resting-state MRI literature". en. In: *BMC Med.* 19.1,  
502 p. 103.

- 503 Shen, Jun et al. (2020). "Network Efficiency Mediates the Relationship Between Vascular  
504 Burden and Cognitive Impairment: A Diffusion Tensor Imaging Study in UK Biobank". en.  
505 en. In: *Stroke* 51.6, pp. 1682–1689.
- 506 Steegen, Sara et al. (2016). "Increasing Transparency Through a Multiverse Analysis". en.  
507 en. In: *Perspect. Psychol. Sci.* 11.5, pp. 702–712.
- 508 Sundaresan, Vaanathi et al. (2019). "Automated lesion segmentation with BIANCA: Im-  
509 pact of population-level features, classification algorithm and locally adaptive thresh-  
510 olding". en. In: *Neuroimage* 202, p. 116056.
- 511 Tombaugh, Tom N (2004). "Trail Making Test A and B: normative data stratified by age  
512 and education". en. In: *Arch. Clin. Neuropsychol.* 19.2, pp. 203–214.
- 513 Tuladhar, Anil M, Ewoud van Dijk, et al. (2016). "Structural network connectivity and cog-  
514 nition in cerebral small vessel disease". en. In: *Hum. Brain Mapp.* 37.1, pp. 300–310.
- 515 Tuladhar, Anil M, Jonathan Tay, et al. (2020). "Structural network changes in cerebral small  
516 vessel disease". en. In: *J. Neurol. Neurosurg. Psychiatry* 91.2, pp. 196–203.
- 517 Tzourio-Mazoyer, Nathalie et al. (2002). "Automated anatomical labeling of activations in  
518 SPM using a macroscopic anatomical parcellation of the MNI MRI single-subject brain".  
519 In: *Neuroimage* 15.1, pp. 273–289.
- 520 Vidaurre, Diego et al. (2018). "Discovering dynamic brain networks from big data in rest  
521 and task". en. In: *Neuroimage* 180.Pt B, pp. 646–656.
- 522 Wardlaw, Joanna M, Colin Smith, and Martin Dichgans (2013). "Mechanisms of sporadic  
523 cerebral small vessel disease: insights from neuroimaging". en. In: *Lancet Neurol.* 12.5,  
524 pp. 483–497.
- 525 Wardlaw, Joanna M, Eric E Smith, et al. (2013). "Neuroimaging standards for research  
526 into small vessel disease and its contribution to ageing and neurodegeneration". en.  
527 In: *Lancet Neurol.* 12.8, pp. 822–838.
- 528 Wardlaw, Joanna M, María C Valdés Hernández, and Susana Muñoz-Maniega (2015). "What  
529 are white matter hyperintensities made of? Relevance to vascular cognitive impair-  
530 ment". en. In: *J. Am. Heart Assoc.* 4.6, p. 001140.
- 531 Xu, Yuanhang et al. (2021). "Altered Dynamic Functional Connectivity in Subcortical Is-  
532 chemic Vascular Disease With Cognitive Impairment". en. In: *Front. Aging Neurosci.* 13,  
533 p. 758137.
- 534 Yeo, B T Thomas et al. (2011). "The organization of the human cerebral cortex estimated  
535 by intrinsic functional connectivity". en. In: *J. Neurophysiol.* 106.3, pp. 1125–1165.

- <sup>536</sup> Yin, Wenwen et al. (2022). "The Clustering Analysis of Time Properties in Patients With  
<sup>537</sup> Cerebral Small Vessel Disease: A Dynamic Connectivity Study". en. In: *Front. Neurol.*  
<sup>538</sup> 13, p. 913241.

Question	Hypothesis	Sampling plan	Analysis plan	Ratio-nale for deciding the sensitivity of the test	Interpretation given different outcomes	Theory that could be shown wrong by the outcome
Is severity of cerebral small disease, quantified by the volume of supratentorial white matter hyperintensities of presumed vascular origin (WMH), associated with time spent in high-occupancy brain states, defined by resting-state functional MRI?	<b>(Primary)</b> Higher WMH volume is associated with lower average occupancy of the two highest-occupancy brain states.	Available <del>subjects</del> participants with clinical and imaging data from the the HCHS (Jagodzinski et al., 2020)	Standardized preprocessing of structural and functional MRI data • automatic quantification of WMH • co-activation pattern analysis • multivariable generalised regression analyses	Tradition	$P < 0.05 \rightarrow$ rejection of the null hypothesis of no association between cSVD and fractional occupancy; $P > 0.05 \rightarrow$ insufficient evidence to reject the null hypothesis	Functional brain dynamics are not related to subcortical ischemic vascular disease.
Is time spent in high-occupancy brain states associated with cognitive impairment, measured as the time to complete part B of the trail making test (TMT)?	<b>(Secondary)</b> Lower average occupancy of the two highest-occupancy brain states is associated with longer TMT-B time.	as above	as above	as above	$P < 0.05 \rightarrow$ rejection of the null hypothesis of no association between fractional occupancy and cognitive impairment; $P > 0.05 \rightarrow$ insufficient evidence to reject the null hypothesis	Cognitive function is not related to MRI-derived functional brain dynamics.

**Table 1 | Study Design Tempate.** Overview of the Scientific Questions addressed in the present study (first column), the two main hypotheses being investigated (second column), and details of the underlying study.

Name of the atlas	#parcels	Reference
Desikan-Killiany	86	Desikan et al., 2006
AAL	116	Tzourio-Mazoyer et al., 2002
Harvard-Oxford	112	Makris et al., 2006
glasser360	360	Glasser et al., 2016
gordon333	333	Gordon et al., 2016
power264	264	Power, Cohen, et al., 2011
schaefer{N}	100	Schaefer et al., 2018
	200	
	400	

AAL: Automatic Anatomical Labelling

**(a) Parcellations**

Design	Reference
24p	Friston et al., 1996
24p + GSR	Macey et al., 2004
36p	Satterthwaite et al., 2013
36p + spike regression	Cox, 1996
36p + despiking	Satterthwaite et al., 2013
36p + scrubbing	Power, Mitra, et al., 2014
aCompCor	Muschelli et al., 2014
tCompCor	Behzadi et al., 2007
AROMA	Pruim et al., 2015

GSR: Global signal regression, AROMA: Automatic Removal of Motion Artifacts

**(b) Confound regression strategies, adapted from (Ciric, Wolf, et al., 2017)**

**Table 2 | Multiverse analysis.** Overview over different brain parcellations and confound regression strategies implemented using xcpEngine (Ciric, Rosen, et al., 2018). A total of  $9 \times 9 = 81$  analytical combinations were explored to assess the robustness of our results with respect to these processing choices.

<b>N = 1,651</b>	
<i>Demographics (no Missing n (%))</i>	
<i>Age, yr</i>	
Median (IQR)	66 (59 – 72)
<i>Sex</i>	
Male	940/1651 (57%)
Female	711/1651 (43%)
<i>Cardiovascular risk factors</i>	
<i>Hypertension</i>	
Present	1177/1611 (73.1%)
Missing n (%)	85 (5.1%)
<i>Diabetes</i>	
Present	157/1566 (10%)
Missing n (%)	40 (2.4%)
<i>Smoking</i>	
Present	200/1360 (14.7%)
Missing n (%)	201 (12.9%)
<i>Hyperlipidaemia</i>	
Present	426/1578 (27%)
Missing n (%)	73 (4.4%)
<i>Cognitive test results</i>	
<i>MMSE, # (max. 30)</i>	
Median (IQR)	28 (27 – 29)
Missing n (%)	129 (7.8%)
<i>Vocabulary (MWT-B), # (max. 37)</i>	
Median (IQR)	32 (30 – 34)
Missing n (%)	295 (18%)
<i>Word recall, # (max. 10)</i>	
Median (IQR)	8 (6 – 9)
Missing n (%)	180 (11%)
<i>Animal Naming</i>	
Median (IQR)	24 (20 – 29)
Missing n (%)	116 (7.0%)
<i>TMT-A, seconds</i>	
Median (IQR)	38 (31 – 48)
Missing n (%)	144 (8.7%)
<i>TMT-B, seconds</i>	
Median (IQR)	83 (65 – 110)
Missing n (%)	162 (9.8%)
<i>History</i>	
<i>Diagnosed dementia</i>	
Present	6/1645 (0.4%)
Missing n (%)	6 (0.4%)
<i>Years of education</i>	
Median (IQR)	13 (12 – 16)
Missing n (%)	34 (2%)

**Table 4 | Descriptive statistics of the study population.** Data are presented as median (interquartile range) or count (percentage) of non-missing items, as appropriate. Number of percentage of missing items are reported separately.

N = 1,651	
WMH volume <sup>1</sup> , mL	
Total	1.05 (0.47 – 2.37), 9 Z
Periventricular	0.94 (0.43 – 2.04), 9 Z
Deep	0.10 (0.03 – 0.37), 344 Z
Motion during rs-fMRI	
Framewise displacement, mm	0.21 (0.15 – 0.63)
RMSD, mm	0.086 (0.058 – 0.12)
DVARS	27.8 (24.3 – 31.8)
Fractional occupancy, %	
DMN+	24.8 (20.8 – 28.0)
DMN-	24.0 (20.0 – 28.0)
S3	18.4 (15.2 – 22.4)
S4	16.8 (12.8 – 20.8)
S5	15.2 (12.0 – 19.2)

<sup>1</sup>Number of zero values indicated by Z

**Table 5 | Structural and functional imaging characteristics.** Data are presented as median (interquartile range). Supratentorial WMH volumes were obtained by semiautomatic segmentation of FLAIR images using a BINACA/LOCATE-based  $k$ -nearest neighbours algorithm and stratified by their distance to the lateral ventricles (<10 mm, periventricular; >10 mm, deep). Motion parameters were estimated during fMRIprep processing of BOLD scans. Fractional occupancies were calculated by assigning individual BOLD volumes to one of five discrete brain states defined by k-means clustering-based co-activation pattern analysis. Two high-occupancy states are labelled DMN+ and DMN- in view of their network connectivity profiles as shown in Figure 6.

	Estimate	P	95%-CI
Intercept	0.24	<0.0001	0.21 – 0.27
WMH, per 5.1-fold increase <sup>1</sup>	0.94	<0.0001	0.92 – 0.96
Age, per 10 years	1.04	0.001	1.01 – 1.06
Female sex	1.12	<0.0001	1.09 – 1.16
$\mathbf{1}_{\{\text{WMH}=0\}}$	0.93	0.477	0.75 – 1.14

<sup>1</sup> Interquartile ratio 2.37/0.468 = 5.06

**Table 7 | Association between time-spent in high-occupancy DMN-related brain states and WMH volume adjusted for age and sex.** Beta regression table estimated from  $n = 1651$  independent participants using the model equation  $\text{FO}^{\text{high}} \sim \log \text{WMH}^+ + \mathbf{1}_{\{\text{WMH}=0\}} + \text{age} + \text{sex}$ .

	Estimate	P	95%-CI
Intercept	53.41	< 0.0001	42.7 – 66.8
FO <sup>high</sup> , per 5%	0.98	0.0116	0.96 – 0.99
WMH, per 5.1-fold increase <sup>1</sup>	1.01	0.367	0.98 – 1.05
Age, per 10 years	1.18	<0.0001	1.15 – 1.21
Female sex	0.99	0.666	0.95 – 1.03
Education, per year	0.97	<0.0001	0.97 – 0.98
<b>1<sub>{WMH=0}</sub></b>	0.97	0.398	0.92 – 1.03

<sup>1</sup> Interquartile ratio 2.37/0.468 = 5.06

**Table 9 | Association between TMT-B and time spent in high-occupancy DMN-related brain states adjusted for age, sex, WMH volume and years of education.** Gamma regression table

estimated from  $n = 1483$  independent participants using the model equation

$TMT-B \sim FO^{high} + \log WMH^+ + 1_{\{WMH=0\}} + \text{age} + \text{sex} + \text{educationyears}$ .

# Appendix 1

539

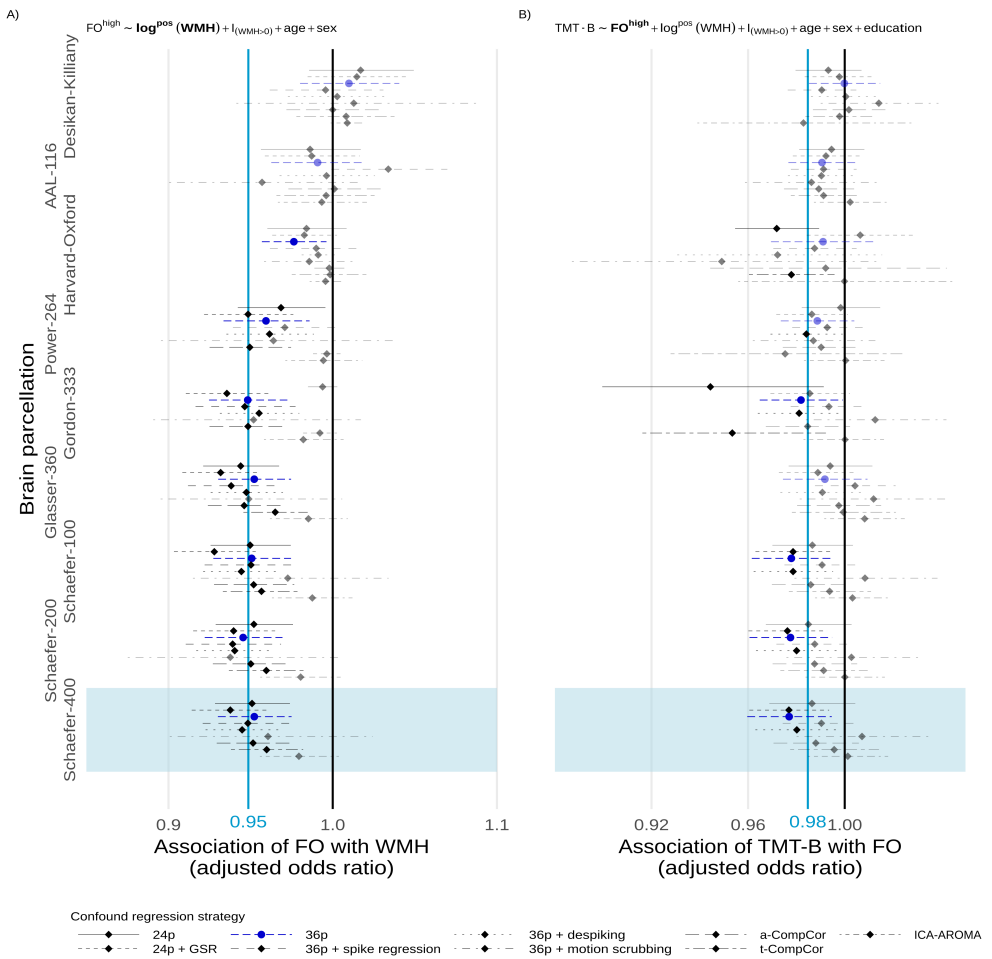
## Supplementary results

540

### Deep and periventricular WMH

541

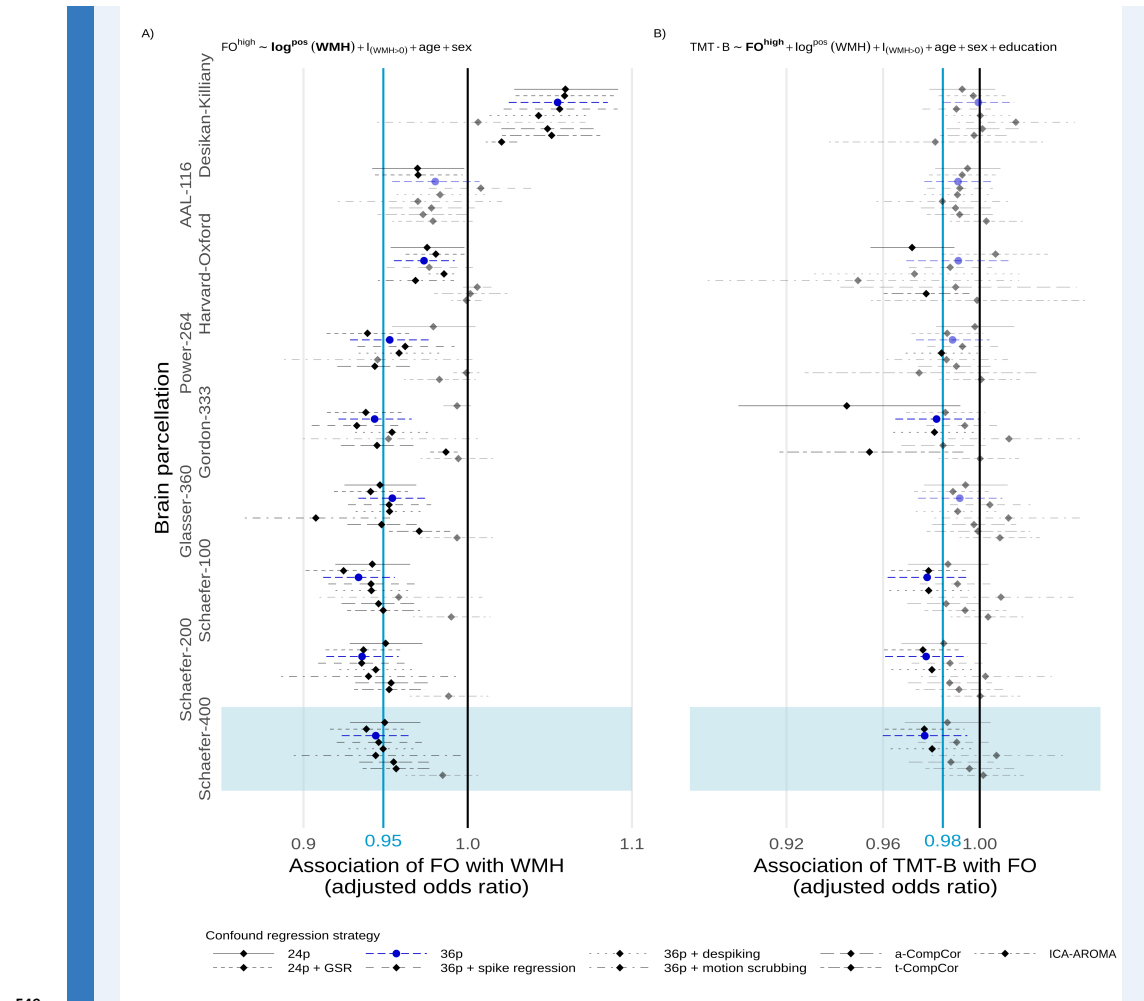
542 Here we present, in analogy to Figure 5, the results of the multiverse analyses of  
 543 the association between cSVD burden, FO of DMN-related states, and executive  
 544 function, when cSVD is operationalized as the volume of deep or periventricular  
 545 white matter hyperintensities, respectively.



546 Appendix 1—figure 1 Multiverse analysis, deep WMH

547

548



549  
550

#### Appendix 1—figure 2 Multiverse analysis, periventricular WMH

552  
553  
554  
555  
556

### Motion parameters

We also present, in analogy to Tables 7 and 9, regression tables for the association between time spent in DMN-related brain states (FO) and WMH volume, and between TMT-B and FO, adjusted for DVARS, RSMD and framewise displacement, in addition to age, sex and, in the latter case, years of education.

	Estimate	P	95%-CI
Intercept	0.32	<0.0001	0.28 – 0.36
WMH, per 5.1-fold increase <sup>1</sup>	0.96	0.0004	0.94 – 0.98
Age, per 10 years	1.01	<0.0001	1.00 – 1.01
Female sex	1.11	<0.0001	1.08 – 1.15
$\mathbf{I}_{(\text{WMH}=0)}$	0.91	0.3552	0.74 – 1.11

DVARS	0.98	<0.0001	0.98 – 0.99
RMSD	28.29	0.0055	2.67 – 299.84
Framewise displacement	0.16	0.0112	0.04 – 0.66

557  $^1$  Interquartile ratio 2.37/0.468 = 5.06

558 **Appendix 1—table 2** Association between time-spent in high-occupancy DMN-related  
560 brain states and WMH volume adjusted for age, sex, and **motion parameters**

	Estimate	P	95%-CI
Intercept	46.83	<0.0001	36.74 – 59.72
FO <sup>high</sup> , per 5%	0.71	0.0718	0.49 – 1.03
WMH, per 5.1-fold increase <sup>1</sup>	1.01	0.3414	0.98 – 1.04
Age, per 10 years	1.02	<0.0001	1.01 – 1.02
Female sex	1.00	0.8171	0.96 – 1.04
Education, per year	0.97	<0.0001	0.97 – 0.98
1 <sub>{WMH=0}</sub>	0.96	0.7581	0.73 – 1.29
DVARS	1.01	0.0001	1.00 – 1.01
RMSD	0.31	0.4695	0.01 – 7.45
Framewise displacement	1.08	0.9322	0.16 – 7.13

561  $^1$  Interquartile ratio 2.37/0.468 = 5.06

562 **Appendix 1—table 4** Association between TMT-B and time spent in high-occupancy  
563 DMN-related brain states adjusted for age, sex, WMH volume and years of education, and  
565 **motion parameters**